RESEARCH ARTICLE

A Physics-Informed Neural Network-Based Waveguide Eigenanalysis

MD RAYHAN KHAN[1], **(Member, IEEE), CONSTANTINOS L. ZEKIOS**[1], **(Senior Member, IEEE),**
SHUBHENDU BHARDWAJ[2], **(Member, IEEE),**
AND STAVROS V. GEORGAKOPOULOS[1], **(Senior Member, IEEE)**

[1]Department of Electrical and Computer Engineering, Florida International University, Miami, FL 33174, USA
[2]Department of Electrical and Computer Engineering, University of Nebraska–Lincoln, Lincoln, NE 68588, USA

Corresponding author: Md Rayhan Khan (mkhan118@fiu.edu)

ABSTRACT This work presents a deep neural network (DNN)-based approach for identifying the modal field distributions of closed non-radiating waveguides. Specifically, physics-informed neural networks (PINNs) are used to solve the Helmholtz partial differential equation. The PINN architecture includes incorporation of boundary conditions and selection of initial conditions to obtain required modes inside the waveguides. In this paper, furthermore, the use of this method is illustrated for waveguides consisting of inhomogeneous and anisotropic media, where we apply a domain decomposition-based deep learning method. Our approach successfully identifies all eigenmode distributions with an error of less than -12 dB as compared to analytical and full-wave simulation results. Notably, we further enhance the efficiency of our approach by utilizing transfer learning, achieving a 23 times reduction in solution time. Our results demonstrate PINNs as an alternative to traditional methods in accurately calculating waveguide modal field distributions and its applicability to other partial differential equation based EM problems.

INDEX TERMS Physics-informed neural network, deep learning, domain decomposition, transfer learning, eigenanalysis, waveguides.

I. INTRODUCTION

Deep neural networks have demonstrated their use towards approximating arbitrary functions for modeling and prediction in different fields [1], [2]. However, in practice, they are often used as black-box techniques which can disregard the underlying physics. Despite their success in solving challenging problems in image processing [3], [4], healthcare [5], [6], autonomous driving [7], [8], seismology [9], materials science [10], etc., they are reliant on pre-existing data. Various factors can hinder their performance, such as the need for large amounts of high-quality training data, observational bias, inadequate feature selection, incorrect data labeling, and extrapolation issues [11], [12].

To address the limitations of data-based solutions for physics problems, physics-informed neural networks

The associate editor coordinating the review of this manuscript and approving it for publication was Sotirios Goudos.

(PINNs) have emerged in [13] and further expanded in [14] and [15]. PINNs offer a direct solution to the physics problem by combining a neural network with underlying partial differential equations (PDEs). Therefore, in contrast with data-driven techniques, PINNs directly solve the PDEs under the constraints of boundary conditions with limited or no prior data. This allows the solution to be trustworthy, interpretable, physics accurate, and generalizable to the class of PDEs considered. Due to these distinct features, PINN-based problem-solving approaches are being studied in physical sciences, including fluid mechanics [16], [17], [18], [19], [20], solid mechanics [21], [22], [23], chemistry [24], [25], and geoscience [26], [27].

In the fields of antennas and microwave engineering, data-driven deep learning, although applied extensively, presents computational challenges due to the need for thorough numerical analysis to generate sufficient training data. However, since the governing physical laws for electromagnetic
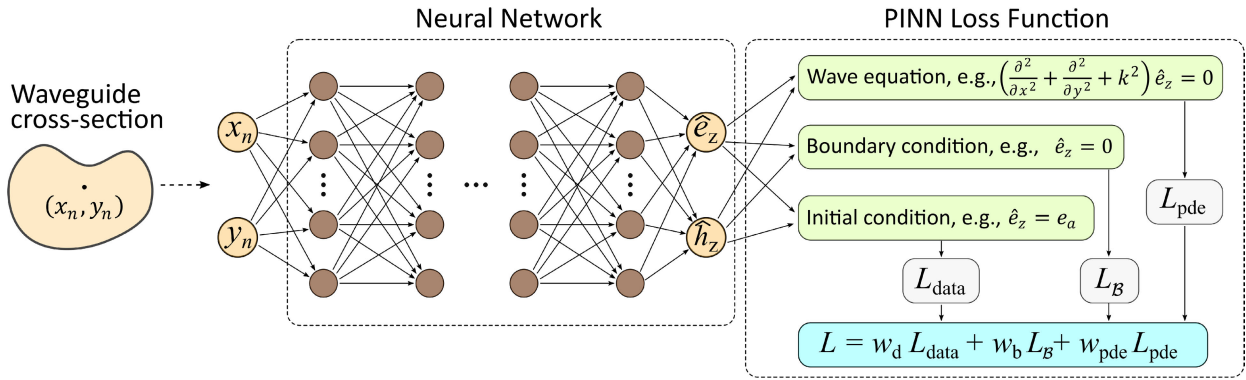
FIGURE 1. A brief overview of the PINN architecture for eigenanalysis of waveguides in 2D: A neural network with input, (x_n, y_n) and output, (e_z, h_z) is trained by minimizing a loss function formulated using the governing wave PDE, boundary, and initial conditions. The neural network loss, L, is a weighted sum of the PDE loss, L_{pde}, initial and/or boundary condition loss, $L_{\mathcal{B}}$, and data point loss, L_{data}, w_{pde}, w_b, and w_{data} are the respective weights.

(EM) problems are well-known, PINNs are a promising candidate for analyzing EM structures. Recent research has shown significant attention from EM researchers in utilizing PINNs for various EM problems, such as time-domain EM analysis [28], [29], electrostatic problems [30], inverse design [31], [32], forward scattering [33], and inverse scattering [34], [35].

In this work, we aim to expand and augment the use of PINNs in the field of electromagnetics by introducing a novel data-free PINN-based approach that determines the modal field distributions in the cross-section of closed waveguides by solving the Helmholtz wave equation. Waveguides are essential components in optical and radio frequency (RF) systems [36], [37], [38] and particle acceleration [39], [40], and determining their eigenmodes and eigenfunctions is crucial for their design and analysis. Our approach involves minimizing a loss function that integrates the wave equation and necessary electromagnetic boundary and initial conditions (BCs, ICs) while training a deep neural network. In addition, we develop domain decomposition-based deep learning methods to accurately model highly inhomogeneous and anisotropic waveguides. Notably, we investigate computational aspects, including the selection of sampling frequency and its impact on computation time. We also address challenges encountered, such as identifying multiple waveguide modes and understanding the impact of neural network architecture on the method's effectiveness. Also, we focus on how to further enhance the computational efficiency of our approach by utilizing transfer learning. To validate our approach, we examine various waveguide designs, and compare our results with both analytical solutions and numerical simulations. Our comparisons demonstrate the approach's effectiveness, with average errors as low as -18 dB, or 1.6%, or less.

The manuscript is organized as follows. Section II introduces the proposed PINN method. Section III demonstrates the ability of PINN to accurately perform waveguide analysis, and Section IV addresses the challenges PINN encounters when solving such problems. Section V presents transfer learning, and demonstrates its efficiency in several waveguide scenarios. Finally, Section VI presents our conclusions.

II. PINN-BASED WAVEGUIDE EIGENANALYSIS
This section briefly reviews the core concepts of physics-informed deep learning, and introduces the proposed method for using PINNs to find the modal field distributions of waveguides.

A. PINN OVERVIEW FOR PDE SOLUTION
The concept of PINN was initially proposed as an alternative method for solving PDEs, specifically boundary value problems, by leveraging the capabilities of neural networks [15]. In a general form, a one-dimensional boundary value problem involving PDEs defined in the domain, $\Omega \subset \mathbb{R}^n$ can be expressed as follows:

$$\mathcal{F}[u(x)] = f(x) \quad x \text{ in } \Omega,$$
$$\mathcal{B}[u(x)] = g(x) \quad x \text{ in } \partial\Omega, \tag{1}$$

where, x, $\mathcal{F}$, $f(x)$, and $u(x)$ are input variable ($x=\{x_1, \ldots, x_n\}$), differential operator, source function and the unknown solution, respectively. Operator $\mathcal{B}$ represents initial (IC) or the boundary conditions (BC), and $g(x)$ is the boundary function.

The conditions of (1) are implemented in a surrogate PINN framework, with its trainable parameters, θ. To elaborate, PINN generates an output, $\hat{u}(x)$, to approximate the target function, $u(x)$, i.e., $\hat{u}(x) \approx u(x)$. This can be achieved by reducing composite loss term by neural network optimization process. A loss term can be formulated by using the weighted sum of the PDE loss, L_{pde}, initial and/or boundary condition loss, $L_{\mathcal{B}}$, and data point loss, L_{data} during the neural network training. The neural network architecture used in this paper for a two-dimensional case (with variables x, y) is shown in Fig. 1.

A distinct advantage here is that unlike traditional numerical techniques used for solving PDEs, such as finite element analysis (FE), finite difference analysis (FD), and
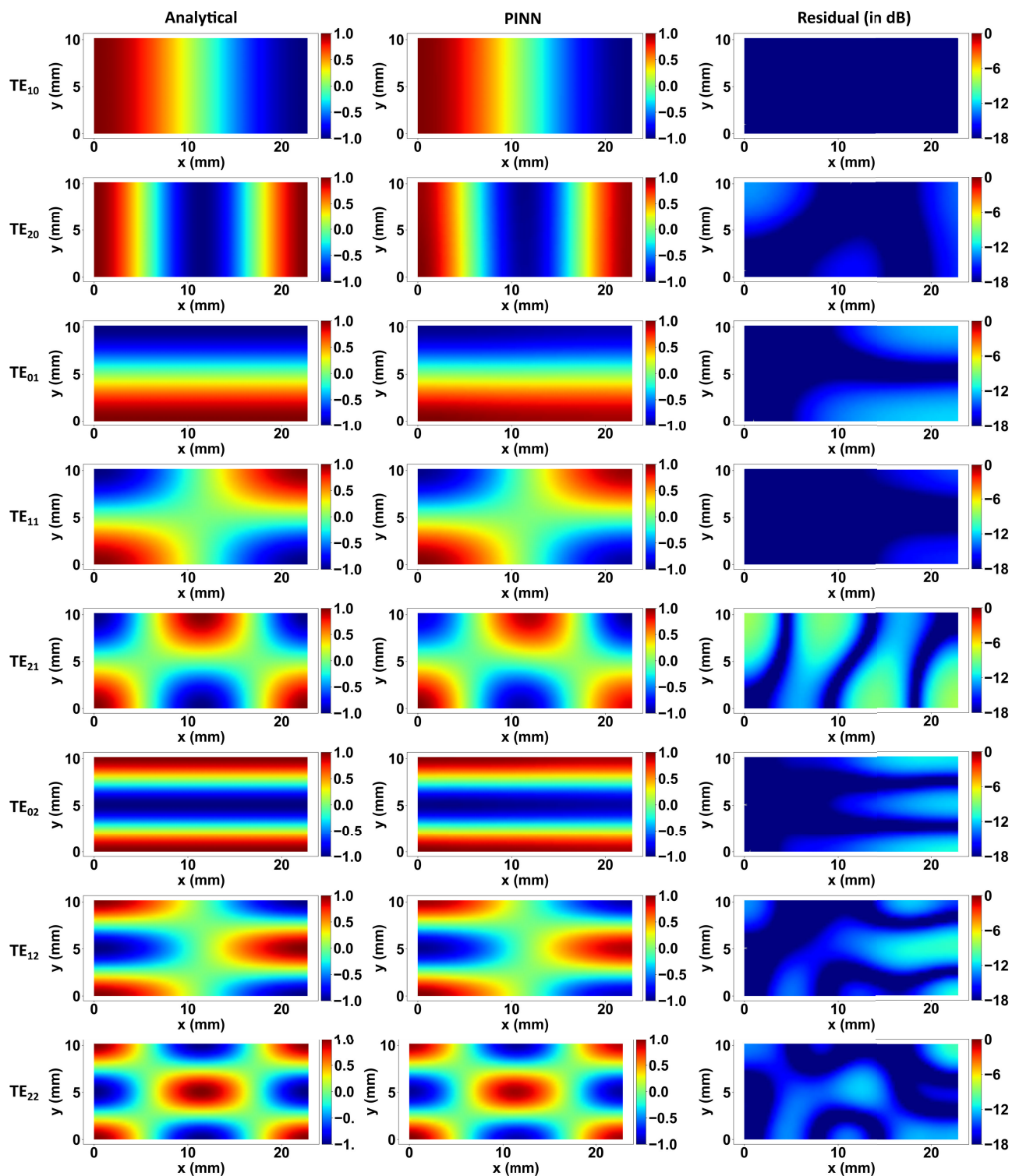
FIGURE 2. Magnetic field distribution (h_z) of the first eight TE_{mn} modes (ordered in the increasing order of the wavenumber) of a WR90 rectangular waveguide.

boundary element analysis (BE), PINNs do not require mesh elements, which can be computationally expensive for high-dimensional problems. More details on PINNs can be found in [41].

B. WAVEGUIDE PDE, BOUNDARY CONDITIONS AND INITIAL CONDITION SELECTION

In this study, 2-D waveguide structures with varying cross-section shapes, material properties, and material distributions

are investigated via the proposed PINN architecture. In a waveguide filled with a homogeneous, isotropic medium, the field distributions are described by the well-known Helmholtz wave equation [42],

$$\left(\frac{\partial^2}{\partial x^2} + \frac{\partial^2}{\partial y^2} + k^2\right)u(x, y) = 0 \quad u \text{ in } \Omega, \tag{2}$$

where, $u(x, y)$ is the z-component of the electric field (i.e., e_z), or the magnetic field (i.e., h_z), for the case of TM and TE modes, respectively, and k is the wavenumber. For each case, appropriate Dirichlet and Neumann boundary conditions should be considered as well. For example, the tangential electric field, $\vec{E}_{tan}$, needs to be zero at perfectly conductive surfaces $\partial\Omega$.

Since the current problem is a source-free PDE, an initial value of u at an arbitrary point should be selected for a non-trivial PINN convergence. This condition applied on the unknown function provides an additional initial condition. Here, $\hat{u}(x_a, y_a) = u_a$ is introduced at a chosen point (x_a, y_a). Selection of $\hat{u}(x_a, y_a) = u_a$ and (x_a, y_a) can be further used to converge the solution to a specific mode for a given wavenumber, k. Here, $u_a=1$ is an arbitrarily chosen, and it normalizes the output field distribution in the cross-section around the selected value of $u(x_a, y_a) = u_a$.

C. PINN NETWORK ARCHITECTURE

The PINN network architecture chosen for the solution of the problems discussed in this paper is derived from the general architecture shown in Fig.1. The inputs to the neural network is a series of spatial coordinates in the waveguide cross-section and the output is the corresponding value of the field variables, e.g., electric and/or magnetic field, at the corresponding spatial points. We select the neural network with two inputs, each corresponding to one of the dimensions in the 2-D domain, one output, and 3 hidden layers with 50 neurons in each layer. In some cases, the number of input and the output nodes are varied as explained wherever required in the paper. Moreover, we use the Xavier initialization method [43] to initialize the neural network weights, and the hyperbolic tangent function as an activation function. During training, a stochastic gradient descent method, namely Adam [44], is used to optimize the weights and the biases of the neural network. The selection of hidden layers and the number of neurons in the layers is chosen based on the complexity of the expected field as inspired by previous architectures [41]. The selection of hyper-parameters is based on our own investigation in this area, and many sets of hyper-parameters can provide similar performance. Mean squared error (MSE) is chosen as the method of averaging the error and loss across the domain. Equal weights are chosen for different loss components L (see Fig. 1) in the surrogate network.

Due to the use of a PINN-inspired architecture, the algorithm does not require any preliminary data on mode distribution. Therefore, with the knowledge of the wave

TABLE 1. Number of sample points considered while solving the waveguide problems discussed in Section III using PINN.

Waveguide problem	Inside domain	On boundary	Total
Conventional hollow waveguides (Fig. 2, Section III-A)	3071	1002	4073
Homogeneously filled with isotropic media arbitrary cross-section waveguides (Fig. 4(a), Section III-B)	3000	1052	4052
Homogeneously filled with isotropic media arbitrary cross-section waveguides (Fig. 4(b), Section III-B)	3000	1056	4056
Conventional waveguides filled homogeneously with anisotropic media (Fig. 5, Section III-C)	3071	1002	4073
Conventional waveguides filled inhomogeneously with isotropic media (Fig. 6, Section III-D)	2764	222	2986

number, k, and the domain, the field distribution function is predicted.
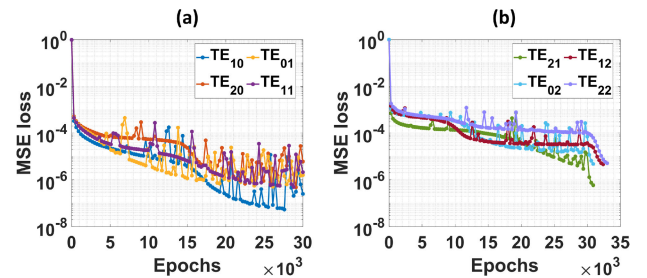

FIGURE 3. (a)-(b) Neural network training convergence curves (total MSE loss vs. epochs) for the eight TE_{mn} modes shown in Fig. 2.

III. PINN APPLICATION SCENARIOS

To rigorously demonstrate the solution of waveguide eigenmode problems and to assess the performance of the PINN architecture in different scenarios, four scenarios are selected to show the versatility of the proposed method of solution: (a) conventional hollow waveguides (e.g., waveguides with a rectangular cross-section) in Section III-A, (b) waveguides of an arbitrary cross-section homogeneously filled with isotropic media in Section III-B, (c) conventional waveguides homogeneously filled with anisotropic media in Section III-C, and (d) conventional waveguides inhomogeneously filled with isotropic media in Section III-D. The field distributions obtained using PINN are compared to analytical (when available) and numerical simulations.

A. CONVENTIONAL HOLLOW WAVEGUIDES

We first study a WR90 rectangular waveguide with cross-section of 22.86 mm $\times$ 10.16 mm, where the PINN architecture is employed to find the magnetic field $h_z(x, y)$, of the first N ($N = 10$) TE_{mn} modes. For this discussion,

TABLE 2. Summary of error values reported in literature for machine learning algorithms applied to electromagnetic problems.

Reference	Error	
	Minimum	Maximum
Zhang et al., [29] (2021)	Relative error of 8.81×10^{-4} or -30.5 dB	Relative error of 5.51×10^{-3} or -22.6 dB
Khan et al., [30] (2022)	Mean absolute relative error of 1.21×10^{-3} or -29 dB	Mean absolute relative error of 1.41×10^{-2} or -18.5 dB
Saba et al., [33] (2022)	Relative error of 3.4×10^{-3} or -24.7 dB	Relative error of 4.6×10^{-2} or -13.37 dB
Chen et al., [35] (2020)	L^2 error of 0.51% or -23 dB	L^2 error of 5% or -13 dB
This work	Residual error of 3.16×10^{-4} or -35 dB	Residual error of 1.25×10^{-1} or -9 dB

wavenumber, k, is set equal to the cut-off wavenumber [42]. Notably, uniformly spaced points, with sample numbers as outlined in Table 1, are used for the PINN training. For metallic boundaries, Neumann boundary conditions are applied. We also set an initial single point field value as an initial condition to avoid a non-trivial convergence. This value can be chosen arbitrarily and was chosen to be $h_z = 1$ at $(x, y) = (0, 0)$. Fig. 2 compares the first eight TE field distributions obtained using the analytical expression provided in [42], and the distribution predicted by the PINN. As we can see, our PINN achieves very good prediction accuracy when compared to similar works (see Table 2), with a residual error that is smaller than -12 dB[1] in most cases (the minimum error is -35 dB). Notably, the solution time for evaluating each mode of operation is approximately 70 to 80 seconds. Fig. 3 shows the training loss for all the TE$_{mn}$ modes; these results indicate very rapid convergence within a few thousand epochs.

B. ARBITRARY CROSS-SECTION WAVEGUIDES FILLED HOMOGENEOUSLY WITH ISOTROPIC MEDIA

In our second example, we consider eigenmodes of waveguides with arbitrary cross-sections, as shown in Figs. 4(a)-4(b). In this case, (2) is solved for TM mode distributions (i.e., $u = e_z$), and the wavenumber, k, is found by the expression, $\sqrt{k_0^2 - \beta^2}$, where k_0 is the free-space wavenumber and β is the phase constant. For this example, Dirichlet BCs are applied. To train the PINN, randomly sampled points, with sample numbers as shown in Table 1, are chosen for the geometries in Figs. 4(a)-4(b). In addition, we apply the initial condition of $e_z = 1$ at $(x, y) = (9, 6)$ for the geometry shown in Fig. 4(a), and $e_z = 1$ at $(x, y) = (12, 8)$ for the geometry shown in Fig. 4(b). Figs. 4(a)-4(b) compare the field distributions of the TM modes at 28 GHz calculated by eigenanalysis in ANSYS HFSS, and PINN.

[1]The residual error (in dB) is calculated using the following expression: $10 \cdot log_{10}(|\hat{u} - u|)$. Both $\hat{u}$ and u are normalized.

As we can see, our PINN, similar to the previous examples, achieves very good prediction accuracy, with a residual error that is smaller than -12 dB. Notably, we train our PINN using both the Adam and L-BFGS optimizer [45], requiring approximately 79 seconds, and 101 seconds for the waveguides in Fig. 4(a), and 4(b), respectively, using the same workstation as before.
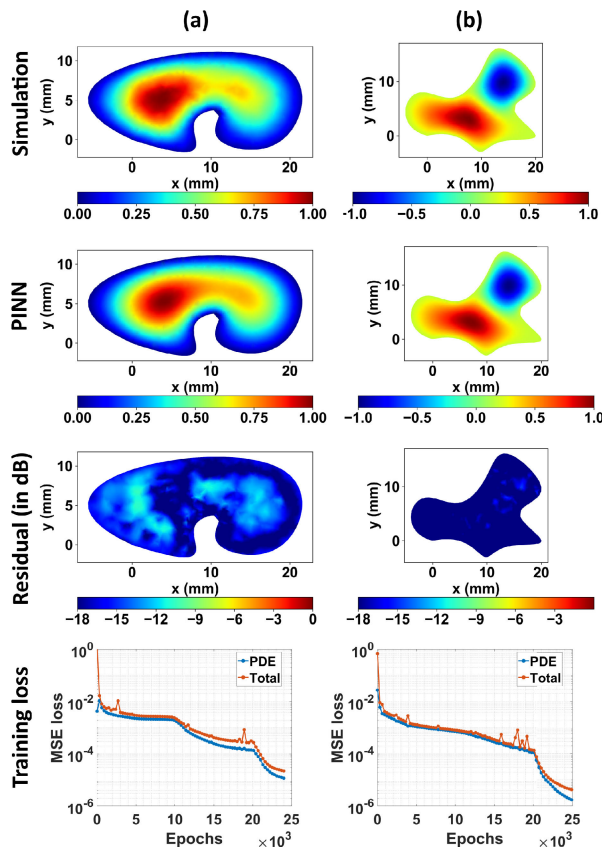

FIGURE 4. Modal field distributions for two arbitrarily shaped cross-section waveguides found by the PINN method are compared with the numerical simulation results. PINN training loss curves for the two cases are also shown. (a) Results for the first waveguide shape. (b) Results for the second waveguide shape.

C. CONVENTIONAL WAVEGUIDES FILLED HOMOGENEOUSLY WITH ANISOTROPIC MEDIA

In our next example, we use PINN to find both the TE and TM modes of a rectangular waveguide homogeneously filled with an anisotropic medium. Specifically, we assume a WR90 waveguide filled with a biaxially anisotropic medium (e.g., $\epsilon_r = \begin{bmatrix} \epsilon_x & 0 & 0 \\ 0 & \epsilon_y & 0 \\ 0 & 0 & \epsilon_z \end{bmatrix}$). Notably, in this case, in contrast to the previous examples, we reformulate the PDEs [46] as in (3), and (4). Notably, $k_{tx} = \omega^2 \mu \epsilon_x - k_z^2$, and $k_{ty} = \omega^2 \mu \epsilon_y - k_z^2$. The electric field, e_z, and magnetic field, h_z, are coupled as long as $k_{tx} \neq k_{ty}$. To model our waveguide, we use a hypothetical medium of electric permittivity, $\epsilon_r = \begin{bmatrix} 2 & 0 & 0 \\ 0 & 4 & 0 \\ 0 & 0 & 6 \end{bmatrix}$. For this case, the scalar wave equation takes the
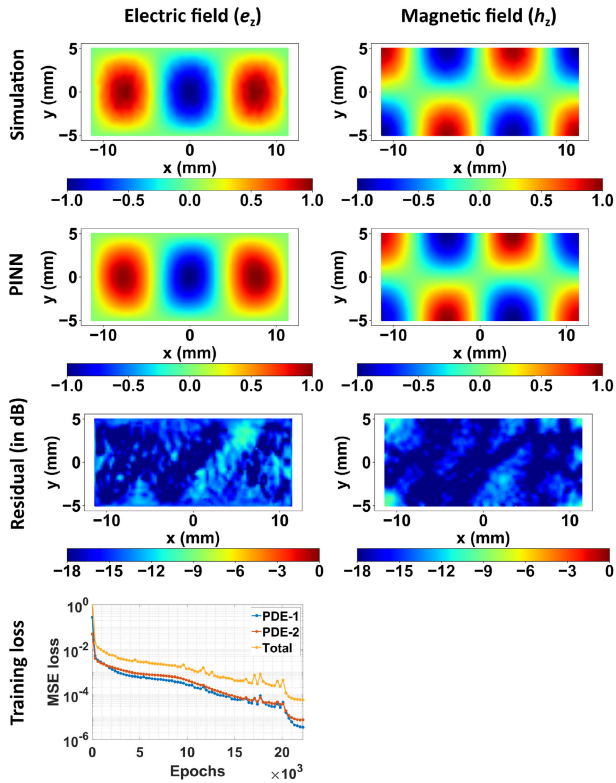
FIGURE 5. Eigenmode electric field (TM mode) and magnetic field (TE mode) distributions for a WR90 waveguide filled with a hypothetical biaxially anisotropic medium, found by the PINN method, are compared with traditional numerical simulation results. Also, the PINN training loss is shown.

our PINN shows impressive prediction accuracy with a residual error of less than −12 dB. Notably, the PINN in this study was trained on our workstation for approximately 200 seconds.
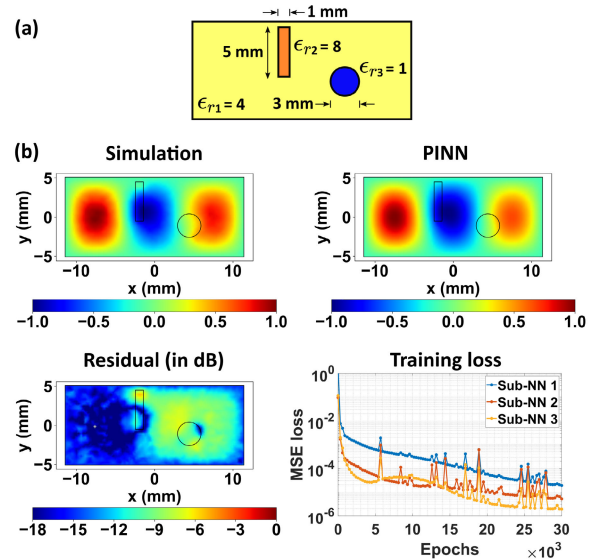

FIGURE 6. (a) Cross-section of an inhomogeneously filled rectangular waveguide. (b) Electric field (TM mode) distribution for an inhomogeneously filled WR90 waveguide, as found by ANSYS HFSS, and by our proposed domain decomposition-based PINN method. Residual error (in dB) and training loss are also shown.

following forms:

$$-\frac{\partial}{\partial x}\left(\frac{\epsilon_x}{k_{tx}^2}\frac{\partial e_z}{\partial x}\right) - \frac{\partial}{\partial y}\left(\frac{\epsilon_y}{k_{ty}^2}\frac{\partial e_z}{\partial y}\right)$$
$$-\frac{k_z}{\omega}\left[\frac{\partial}{\partial x}\left(\frac{1}{k_{tx}^2}\frac{\partial h_z}{\partial y}\right) - \frac{\partial}{\partial y}\left(\frac{1}{k_{ty}^2}\frac{\partial h_z}{\partial x}\right)\right] - \epsilon_z e_z = 0, \quad (3)$$

$$-\frac{\partial}{\partial x}\left(\frac{\mu}{k_{ty}^2}\frac{\partial h_z}{\partial x}\right) - \frac{\partial}{\partial y}\left(\frac{\mu}{k_{tx}^2}\frac{\partial h_z}{\partial y}\right)$$
$$+\frac{k_z}{\omega}\left[\frac{\partial}{\partial x}\left(\frac{1}{k_{ty}^2}\frac{\partial e_z}{\partial y}\right) - \frac{\partial}{\partial y}\left(\frac{1}{k_{tx}^2}\frac{\partial e_z}{\partial x}\right)\right] - \mu h_z = 0. \quad (4)$$

We use uniformly spaced sample points to train the PINN, and the number of sample points considered is shown in Table 1. Notably, to simultaneously predict the two e_z and h_z quantities, in contrast to the previous examples, we add an additional output neuron to the neural network defined previously. Also, both Dirichlet and Neumann BCs are applied, since we are solving for both TM and TE modes, respectively. Moreover, an initial condition of $e_z = -1$ and $h_z = -1$ are applied at $(x, y) = (a/2, b/2)$, and $(x, y) = (0, 0)$, respectively.

Fig. 5 compares the electric and magnetic field distributions obtained from the traditional numerical simulation and those predicted by PINN. Similar to the previous examples,

D. CONVENTIONAL WAVEGUIDES FILLED INHOMOGENEOUSLY WITH ISOTROPIC MEDIA

In this example, we seek the TM mode distributions of an inhomogeneously filled WR90 waveguide. Specifically, as shown in Fig. 6(a), the waveguide is primarily filled with a medium of relative permittivity, $\epsilon_{r1} = 4$. Then, inhomogeneity is imposed by introducing a rectangular and a circular perturbation of $\epsilon_{r2} = 8$, and $\epsilon_{r3} = 1$, respectively. Notably, for a specific eigenmode solution (i.e., a specific phase constant, β), the wavenumber, k, is different in each region, which can be computed by the expression, $\sqrt{\omega^2\mu\epsilon - \beta^2}$. Therefore, the wave equation in (1) needs to be solved considering this spatial variation of k. To efficiently solve this problem, we adopt the domain decomposition-based PINN approach [47], known as *XPINN*. Notably, this specific case of inhomogeneous solution domain can be more effectively addressed using a domain decomposition-based PINN or XPINN, as demonstrated by the authors in [47]. This approach uses parallel neural networks to solve PDEs in the non-overlapping sub-domains. Specifically, separate loss functions are utilized for training the sub-neural networks (sub-NNs). Also, each loss function contains additional interface conditions (e.g., in addition to the boundary and initial conditions) to combine the learning from the sub-NNs. In our case, we consider the residual continuity condition, and the average solution condition at the interfaces (i.e., shared boundaries) while formulating the loss

functions. Detailed instructions on how to formulate these interface conditions in the loss function can be found in [47].

The total number of sample points used in solving this waveguide problem is specified in Table 1. Notably, among the 2764 sample points that are inside the domain, 2464 points (uniform spacing) belong to the larger sub-domain, which is shown using yellow color in Fig. 6(a), and 106 point (uniform spacing), and 194 points (random spacing) belong to the rectangular, and the circular sub-domains, respectively. Notably, for the boundary points, Dirichlet BCs are applied, and the initial condition is set as $e_z = 1$ at $(x, y) = (-7.62, 0)$. Moreover, three sub-NNs are used for these three sub-domains. At each sub-NN, we consider four hidden layers consisting of 50 neurons in each layer. Notably, the training of our PINNs took approximately 900 seconds. Fig. 6(b) shows the TM mode field distribution, as found by ANSYS HFSS and the PINN method, and the residual error, which is approximately -9 dB. Clearly, our results indicate that the XPINN implementation was able to approximate the field distribution in the inhomogeneous waveguide.

IV. PINN CHALLENGES IN WAVEGUIDE EIGENANALYSIS
The preceding examples clearly demonstrate the viability of using PINN for conducting waveguide eigenanalysis. This section focuses on the challenges encountered when employing PINNs for such studies and proposes potential practical solutions. Specifically, we discuss the impact of the number of spatial points considered per wavelength on the solution accuracy and computational time, and show cases where the solution does not converge to the expected result.

A. SOLUTION ACCURACY WITH INCREASING SAMPLE POINTS
In classical numerical methods, fine or coarse mesh can be chosen to obtain the desired level of solution accuracy and computational cost. Here we investigate the impact of increasing sampling points on the solution accuracy. We conduct this study with the understanding that in this mesh-free operation, the sampling time itself remains nearly constant for different cases (unlike meshing time). Cases with parametric variation in sampling points are considered to determine (a) TE$_{11}$ mode H-field distribution for a homogeneous WR90 waveguide, shown in Fig. 2, and (b) TM mode E-field distribution for an inhomogeneous media-filled WR90 waveguide, shown in Fig. 6. Notably, uniformly spaced points along the horizontal and vertical directions are considered.

Fig. 7 shows the average total errors (in dB) and computational times (in seconds) of the PINN computations for different numbers of points per wavelength. As shown in this study, at least 25 points per wavelength (i.e., spacing$<\lambda/25$) are needed to achieve an average error of -12 dB or lower. On the other hand, computational time increases linearly, as expected. This study indicates that, with a specific PINN architecture, increasing the sampling frequency does not improve solution accuracy significantly.
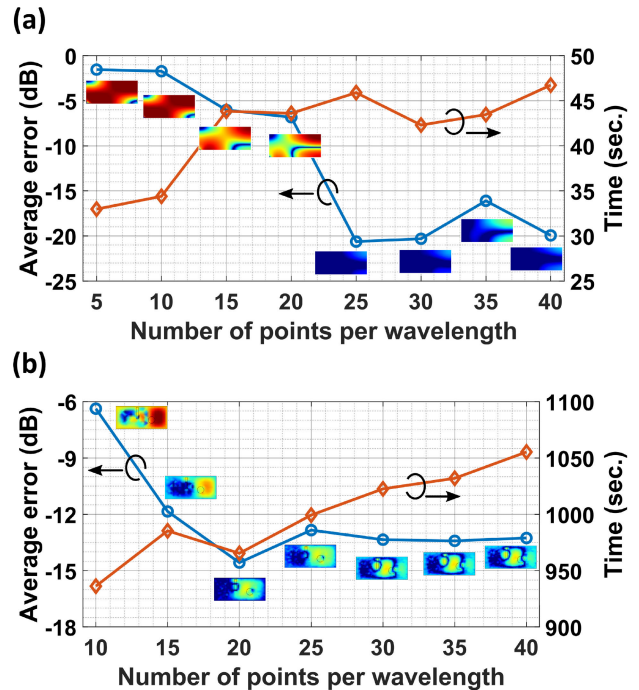

FIGURE 7. Average error (dB) and solution time (seconds) vs. the number of sample points considered per wavelength for: (a) a homogeneous WR90 waveguide in TE$_{11}$ mode (as shown in Fig. 2), and (b) a WR90 waveguide filled with inhomogeneous media in TM mode (as shown in Fig. 6).

B. UNIVERSALITY OF NN-MODELS
Similar to prior NN-algorithms developed in various fields which are based on NN, an architecture is found to most successful only for a specific problem. For example, various problem-specific neural network architectures have been introduced, including XPINN [47] (for domain decomposition-based solution), DeepOnet [48] (for nonlinear operator learning), PhyCRNet [49] (for solving spatiotemporal PDEs), etc.

In this work, we accurately evaluated the eigenmodes for many different cases discussed in Sections III(a)-(c) using the basic PINN model defined at the beginning of Section III. Here, we present a specific case where the basic model does not solve the eigenmode accurately, and, hence, a different model is needed. Specifically, we aim to evaluate one of the TM modes of a WR90 waveguide filled with a material of electric permittivity $\epsilon_{r1} = 4$, and the presence of a thin sliver (of width 0.75 mm or $\lambda_{20GHz}/20$) of a different material with electric permittivity $\epsilon_{r2} = 2$, as shown in Fig. 8(a).

While trying to solve this waveguide problem with the basic PINN model discussed in Section II, the PINN solution, as shown in Fig. 8(c)-left varies significantly (e.g, approximately 45% of the total number of sample points have an error of -9 dB or higher) from the traditional full-wave simulated solution shown in 8(b). Both models are trained using an equal number of points (with 25 points per wavelength). The XPINN solution, as illustrated in Fig. 8(c)-right, exhibits high accuracy, with an average error of -16.53 dB. However, XPINN's improved accuracy comes at the expense
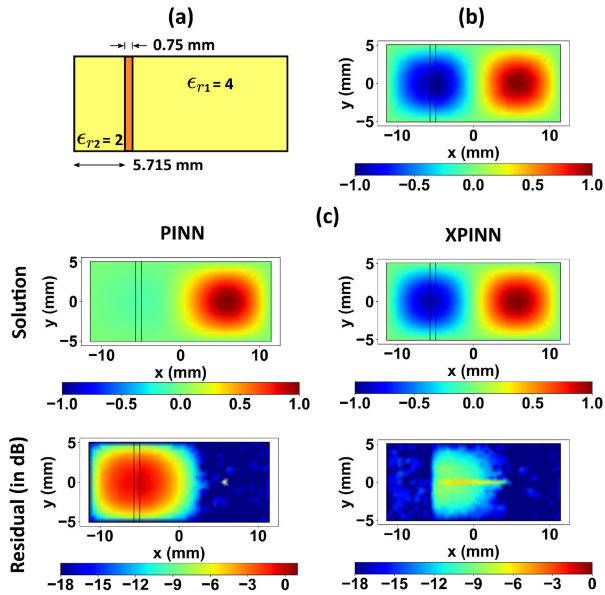
FIGURE 8. (a) A WR90 waveguide geometry filled with a medium of electric permittivity of $\epsilon_r = 4$, including a specific material inhomogeneity (i.e., the thin region marked in orange color, having an electric permittivity, $\epsilon_r = 2$). (b) TM mode field distribution, as obtained using a full-wave solver. (c) Solutions with standard PINN, and domain decomposition-based PINN (or XPINN), and their respective errors.
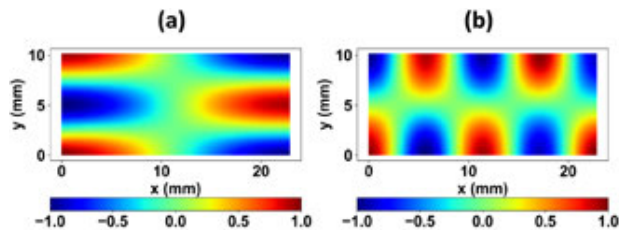

FIGURE 9. Solving a hollow WR90 waveguide using PINN with different initial conditions can yield different modal field distributions. (a) Representative field distribution obtained by using the following initial conditions in separate instances: $u(0, 0) = 1$, $u(0, b) = 1$, and both $u(0, 0) = 1$ and $u(0, b) = 1$. (b) field distribution obtained by using both $u(0, 0) = 1$ and $u(0, b) = -1$ in the same instance. Notably, both (a) and (b) are obtained while setting k at 0.6335.

of increased computation time; specifically, XPINN needed 345 seconds, whereas PINN needed 38 seconds.

C. FORMAL METHOD FOR DETERMINATION OF MULTIPLE MODES

We note that in theory, several modes can be supported by the the same waveguide structure [42]. Notably, the results presented so far demonstrate the ability of PINN to find a specific modal field distribution. However, for a fixed wavenumber, finding different modal field distributions that are supported by the waveguide is indeed possible with a PINN. We achieve this by tuning the initial condition, $u(x_a, y_a)$. For instance, as shown in Fig. 9, different field distributions are obtained for a specific wavenumber ($k = 0.6335$ in this case) using PINN. Here, the mode shown in Fig. 9(a) can be obtained by setting $u(0, 0) = 1$, $u(0, b) = 1$, and both $u(0, 0) = 1$ and $u(0, b) = 1$ in separate

applications of PINN. Also, with the same wavenumber, the mode shown in Fig. 9(b) can be obtained by setting both $u(0, 0) = 1$ and $u(0, b) = -1$.

While we show that, higher or lower order modes can be found using PINNs for a specific waveguide geometry, and a specific wavenumber, the initial condition needs to be adjusted carefully to explore a different mode. Notably, this is a non-standard process, and we leave the discovery of a standardized solution process to find multiple waveguide modes for future research.

V. TRANSFER LEARNING BASED ACCELERATION

Transfer learning is a well-established concept in machine learning, where knowledge gained by a neural network during training for a specific task is leveraged to perform a related task more efficiently [50]. This approach involves the use of optimized weights and biases of a trained neural network as a starting point for another neural network, which leads to faster training and reduced computational effort. Notably, it is analogous to the practice of mesh reuse in popular numerical methods, which accelerates solutions within a frequency band.

In our study, where we employ PINNs to conduct waveguide eigenanalysis, we explore how transfer learning (TL) can expedite the solution of similar waveguide eigenmode problems. To achieve this objective, we utilize PINNs pre-trained with the WR90 waveguide modeled at the beginning of Section III, to model two different example cases; a ridged waveguide and a hexagonal waveguide.

We first consider a PINN that is trained to solve the TM_{11} mode of a vacuum-filled WR90 waveguide, as shown in Fig. 10(a). We also use ANSYS HFSS to calculate the TM modes of the ridged waveguide shown in Fig. 10(b), which has the same overall dimensions along the horizontal and vertical axis. Fig. 10(b) shows the full-wave simulation results. Then, we use the PINN approach to find the same field distribution. We conduct two studies. In the first study, we use the PINN model presented in Section II with a neural network that has not been trained before. This will be called from now on the direct approach. In the second study, we use the PINN model that has already been trained to solve the problem of Fig. 10(a) to calculate the solution of the problem in Fig. 9(b). This will be called from now on the TL approach. Both approaches achieve good accuracy (i.e., low residual error) when compared to the full-wave solution. However, as shown in Fig. 10(d), a significantly faster convergence to a specified MSE loss (i.e., fewer epochs needed to reach a certain MSE) is observed with our second study. This convergence translates to a considerable reduction in computational time. Specifically, the TL approach solves the ridged waveguide for the TM mode approximately 23 times faster than the traditional PINN approach and achieves an MSE loss of 10^{-3}.

For our second example case, we want to evaluate a TE mode of a hexagonal-shaped waveguide. First, we train a PINN to obtain the TE_{10} mode of a WR90 waveguide,
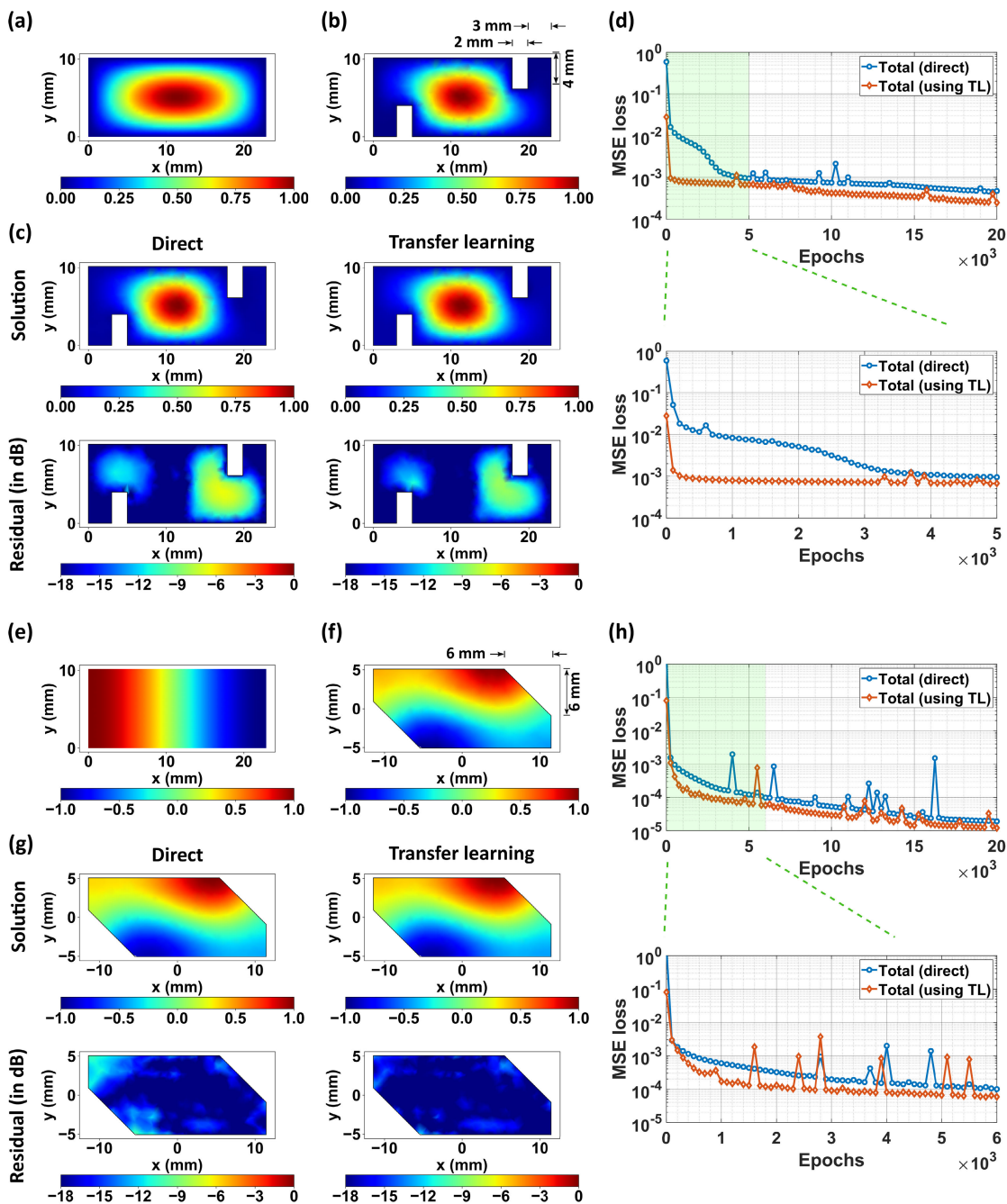
FIGURE 10. Transfer learning-based accelerated PINN solution is presented for two cases. (a) TM_{11} mode field distribution of a WR90 waveguide is shown, obtained by training a PINN. (b) TM mode solution of a ridged waveguide is shown, obtained by using ANSYS HFSS. (c) A comparison between direct solution (i.e., solution using a randomly initialized PINN) and transfer learning solution by using a PINN initialized using the weights of a PINN in Fig. 10(a). (d) By applying transfer learning, a 10^{-3} total MSE loss was achieved approximately 23 times faster compared to solving the problem directly. (e) TE_{10} mode field distribution of a WR90 waveguide is shown, obtained by training a PINN. (f) TE mode solution of a hexagonal waveguide is shown, obtained by using ANSYS HFSS. (g) A comparison between the direct solution and the transfer learning solution is shown for the hexagonal waveguide. (h) By applying transfer learning, a 10^{-4} total MSE loss was achieved approximately 3 times faster compared to the direct PINN solution.

as depicted in Fig. 10(e). We also, conduct full-wave eigenanalysis on the hexagonal-shaped waveguide to use for reasons of validation [see Fig. 10(f)]. As before, two different PINN studies are conducted; the direct and the TL. Fig. 10(g), presents both solutions, along with their respective residual

errors compared to the full-wave solution in Fig. 10(f). Both techniques yield highly accurate solutions. However, as depicted in Fig. 10(h), the TL approach demonstrates faster convergence to a specified MSE loss, resulting in reduced computing time. Notably, when aiming for an MSE loss of

10^{-4}, the TL approach is approximately three times faster than the direct approach.

VI. CONCLUSION

This work presented a neural network-based approach for identifying modal field distributions in closed waveguides, showing promising results across various geometries and material distributions. Utilizing physics-informed neural networks, we solved the Helmholtz partial differential equation while imposing proper boundary and initial conditions to model various waveguide scenarios. Additionally, we addressed computational complexities through domain decomposition-based deep learning methods and discussed the need for tuning the PINN architecture and hyper-parameters for optimal results. Our approach successfully identified several eigenmode distributions under different scenarios, with an error of less than -12 dB, compared to analytical and full-wave simulation results. To further enhance the efficiency of our approach, we utilized transfer learning, resulting in a 23 times reduction in solution time, which is very significant.

Results suggest that the application of PDEs towards electromagnetic problems is possible even under inhomogeneity, non-symmetric boundaries, or anisotropy in the media. While challenges within NNs, such as hyper-parameter selection, and generality continue to be a subject of investigation, PINNs exhibit potential as a compelling alternative to classical solvers for efficiently obtaining waveguide modal field distributions and solving EM problems.

REFERENCES

[1] J. Chai, H. Zeng, A. Li, and E. W. T. Ngai, "Deep learning in computer vision: A critical review of emerging techniques and application scenarios," *Mach. Learn. With Appl.*, vol. 6, Dec. 2021, Art. no. 100134.

[2] M. Reichstein, G. Camps-Valls, B. Stevens, M. Jung, J. Denzler, and N. Carvalhais, "Deep learning and process understanding for data-driven Earth system science," *Nature*, vol. 566, no. 7743, pp. 195–204, Feb. 2019.

[3] E. Moen, D. Bannon, T. Kudo, W. Graf, M. Covert, and D. Van Valen, "Deep learning for cellular image analysis," *Nature Methods*, vol. 16, no. 12, pp. 1233–1246, 2019.

[4] L. Jiao and J. Zhao, "A survey on the new generation of deep learning in image processing," *IEEE Access*, vol. 7, pp. 172231–172263, 2019.

[5] A. Esteva, A. Robicquet, B. Ramsundar, V. Kuleshov, M. DePristo, K. Chou, C. Cui, G. Corrado, S. Thrun, and J. Dean, "A guide to deep learning in healthcare," *Nature Med.*, vol. 25, no. 1, pp. 24–29, 2019.

[6] D. Kaul, H. Raju, and B. K. Tripathy, "Deep learning in healthcare," in *Deep Learning in Data Analytics: Recent Techniques, Practices and Applications*, D. P. Acharjya, A. Mitra, and N. Zaman, Eds. Cham, Switzerland: Springer, 2022, pp. 97–115.

[7] S. Mozaffari, O. Y. Al-Jarrah, M. Dianati, P. Jennings, and A. Mouzakitis, "Deep learning-based vehicle behavior prediction for autonomous driving applications: A review," *IEEE Trans. Intell. Transp. Syst.*, vol. 23, no. 1, pp. 33–47, Jan. 2022.

[8] Y. Li, L. Ma, Z. Zhong, F. Liu, M. A. Chapman, D. Cao, and J. Li, "Deep learning for LiDAR point clouds in autonomous driving: A review," *IEEE Trans. Neural Netw. Learn. Syst.*, vol. 32, no. 8, pp. 3412–3432, Aug. 2021.

[9] S. M. Mousavi and G. C. Beroza, "Deep-learning seismology," *Science*, vol. 377, no. 6607, Aug. 2022, Art. no. eabm4470.

[10] K. Choudhary, B. DeCost, C. Chen, A. Jain, F. Tavazza, R. Cohn, C. W. Park, A. Choudhary, A. Agrawal, S. J. L. Billinge, E. Holm, S. P. Ong, and C. Wolverton, "Recent advances and applications of deep learning methods in materials science," *NPJ Comput. Mater.*, vol. 8, no. 1, pp. 1–26, Apr. 2022.

[11] G. E. Karniadakis, I. G. Kevrekidis, L. Lu, P. Perdikaris, S. Wang, and L. Yang, "Physics-informed machine learning," *Nature Rev. Phys.*, vol. 3, no. 6, pp. 422–440, 2021.

[12] P. Liu, L. Wang, R. Ranjan, G. He, and L. Zhao, "A survey on active deep learning: From model driven to data driven," *ACM Comput. Surv.*, vol. 54, no. 10s, pp. 1–34, Jan. 2022.

[13] I. E. Lagaris, A. Likas, and D. I. Fotiadis, "Artificial neural networks for solving ordinary and partial differential equations," *IEEE Trans. Neural Netw.*, vol. 9, no. 5, pp. 987–1000, Jan. 1998.

[14] M. Raissi, P. Perdikaris, and G. E. Karniadakis, "Physics informed deep learning (Part I): Data-driven solutions of nonlinear partial differential equations," 2017, *arXiv:1711.10561*.

[15] M. Raissi, P. Perdikaris, and G. E. Karniadakis, "Physics-informed neural networks: A deep learning framework for solving forward and inverse problems involving nonlinear partial differential equations," *J. Comput. Phys.*, vol. 378, pp. 686–707, Feb. 2019.

[16] A. M. Roy, R. Bose, V. Sundararaghavan, and R. Arróyave, "Deep learning-accelerated computational framework based on physics informed neural network for the solution of linear elasticity," *Neural Netw.*, vol. 162, pp. 472–489, May 2023.

[17] R. Bose and A. M. Roy, "Invariance embedded physics-infused deep neural network-based sub-grid scale models for turbulent flows," *Eng. Appl. Artif. Intell.*, vol. 128, Feb. 2024, Art. no. 107483.

[18] S. Cai, Z. Mao, Z. Wang, M. Yin, and G. E. Karniadakis, "Physics-informed neural networks (PINNs) for fluid mechanics: A review," *Acta Mechanica Sinica*, vol. 37, no. 12, pp. 1727–1738, Dec. 2021.

[19] Z. Mao, A. D. Jagtap, and G. E. Karniadakis, "Physics-informed neural networks for high-speed flows," *Comput. Methods Appl. Mech. Eng.*, vol. 360, Mar. 2020, Art. no. 112789.

[20] Y. Zhang, H. Fu, Y. Qin, K. Wang, and J. Ma, "Physics-informed deep neural network for inhomogeneous magnetized plasma parameter inversion," *IEEE Antennas Wireless Propag. Lett.*, vol. 21, pp. 828–832, 2022.

[21] A. M. Roy and S. Guha, "A data-driven physics-constrained deep learning computational framework for solving von Mises plasticity," *Eng. Appl. Artif. Intell.*, vol. 122, Jun. 2023, Art. no. 106049.

[22] S. Goswami, M. Yin, Y. Yu, and G. E. Karniadakis, "A physics-informed variational DeepONet for predicting crack path in quasi-brittle materials," *Comput. Methods Appl. Mech. Eng.*, vol. 391, Mar. 2022, Art. no. 114587.

[23] S. Cai, Z. Wang, S. Wang, P. Perdikaris, and G. E. Karniadakis, "Physics-informed neural networks for heat transfer problems," *J. Heat Transf.*, vol. 143, no. 6, Jun. 2021, Art. no. 060801.

[24] W. Ji, W. Qiu, Z. Shi, S. Pan, and S. Deng, "Stiff-PINN: Physics-informed neural network for stiff chemical kinetics," *J. Phys. Chem. A*, vol. 125, no. 36, pp. 8098–8106, Sep. 2021.

[25] H. Chen, E. Kätelhön, and R. G. Compton, "Predicting voltammetry using physics-informed neural networks," *J. Phys. Chem. Lett.*, vol. 13, no. 2, pp. 536–543, Jan. 2022.

[26] S. Karimpouli and P. Tahmasebi, "Physics informed machine learning: Seismic wave equation," *Geosci. Frontiers*, vol. 11, no. 6, pp. 1993–2001, Nov. 2020.

[27] U. B. Waheed, E. Haghighat, T. Alkhalifah, C. Song, and Q. Hao, "PINNeik: Eikonal solution using physics-informed neural networks," *Comput. Geosci.*, vol. 155, Oct. 2021, Art. no. 104833.

[28] O. Noakoasteen, S. Wang, Z. Peng, and C. Christodoulou, "Physics-informed deep neural networks for transient electromagnetic analysis," *IEEE Open J. Antennas Propag.*, vol. 1, pp. 404–412, 2020.

[29] P. Zhang, Y. Hu, Y. Jin, S. Deng, X. Wu, and J. Chen, "A Maxwell's equations based deep learning method for time domain electromagnetic simulations," *IEEE J. Multiscale Multiphys. Comput. Techn.*, vol. 6, pp. 35–40, 2021.

[30] A. Khan and D. A. Lowther, "Physics informed neural networks for electromagnetic analysis," *IEEE Trans. Magn.*, vol. 58, no. 9, pp. 1–4, Sep. 2022.

[31] Y.-Q. Pan, R. Wang, and B.-Z. Wang, "Physics-informed neural networks with embedded analytical models: Inverse design of multilayer dielectric-loaded rectangular waveguide devices," *IEEE Trans. Microw. Theory Techn.*, vol. 72, no. 7, pp. 3993–4005, Jul. 2024.

[32] J.-P. Liu, B.-Z. Wang, C.-S. Chen, and R. Wang, "Inverse design method for horn antennas based on knowledge-embedded physics-informed neural networks," *IEEE Antennas Wireless Propag. Lett.*, vol. 23, pp. 1665–1669, 2024.

[33] A. Saba, C. Gigli, A. B. Ayoub, and D. Psaltis, "Physics-informed neural networks for diffraction tomography," *Adv. Photon.*, vol. 4, no. 6, Nov. 2022, Art. no. 066001.

[34] C. Liu, H. Zhang, L. Li, and T. J. Cui, "Towards intelligent electromagnetic inverse scattering using deep learning techniques and information metasurfaces," *IEEE J. Microw.*, vol. 3, no. 1, pp. 509–522, Jan. 2023.

[35] Y. Chen, L. Lu, G. E. Karniadakis, and L. Dal Negro, "Physics-informed neural networks for inverse problems in nano-optics and metamaterials," *Opt. Exp.*, vol. 28, no. 8, p. 11618, 2020.

[36] E. Rajo-Iglesias, M. Ferrando-Rocher, and A. U. Zaman, "Gap waveguide technology for millimeter-wave antenna systems," *IEEE Commun. Mag.*, vol. 56, no. 7, pp. 14–20, Jul. 2018.

[37] H. I. Song, J.-Y. Lee, H. Won, C.-A. Kim, H. Jin, J. Eu, J. Park, and H.-M. Bae, "E-TUBE: Dielectric waveguide cable for high-speed communication," *Sci. Rep.*, vol. 10, no. 1, pp. 1–8, Oct. 2020.

[38] W. Volkaerts, N. Van Thienen, and P. Reynaert, "10.2 an FSK plastic waveguide communication link in 40nm CMOS," in *IEEE Int. Solid-State Circuits Conf. (ISSCC) Dig. Tech. Papers*, Feb. 2015, pp. 1–3.

[39] I. Staude, C. McGuinness, A. Frölich, R. L. Byer, E. Colby, and M. Wegener, "Waveguides in three-dimensional photonic bandgap materials for particle-accelerator on a chip architectures," *Opt. Exp.*, vol. 20, no. 5, p. 5607, 2012.

[40] K. Oubrerie, A. Leblanc, O. Kononenko, R. Lahaye, I. A. Andriyash, J. Gautier, J.-P. Goddet, L. Martelli, A. Tafzi, K. Ta Phuoc, S. Smartsev, and C. Thaury, "Controlled acceleration of GeV electron beams in an all-optical plasma waveguide," *Light, Sci. Appl.*, vol. 11, no. 1, pp. 1–7, Jun. 2022.

[41] S. Cuomo, V. S. Di Cola, F. Giampaolo, G. Rozza, M. Raissi, and F. Piccialli, "Scientific machine learning through physics–informed neural networks: Where we are and what's next," *J. Sci. Comput.*, vol. 92, no. 3, p. 88, Jul. 2022.

[42] D. M. Pozar, *Microwave Engineering*. Hoboken, NJ, USA: Wiley, 2011.

[43] X. Glorot and Y. Bengio, "Understanding the difficulty of training deep feedforward neural networks," in *Proc. 13th Int. Conf. Artif. Intell. Statist.*, 2010, pp. 249–256.

[44] D. P. Kingma and J. Ba, "Adam: A method for stochastic optimization," in *Proc. 3rd Int. Conf. Learn. Represent.*, 2014, pp. 1–12.

[45] Q. V. Le, J. Ngiam, A. Coates, A. Lahiri, B. Prochnow, and A. Y. Ng, "On optimization methods for deep learning," in *Proc. 28th Int. Conf. Mach. Learn. (ICML)*, 2011, pp. 265–272.

[46] J.-M. Jin, *The Finite Element Method in Electromagnetics*. Hoboken, NJ, USA: Wiley, 2015

[47] A. D. Jagtap and G. E. Karniadakis, "Extended physics-informed neural networks (XPINNs): A generalized space-time domain decomposition based deep learning framework for nonlinear partial differential equations," *Commun. Comput. Phys.*, vol. 28, no. 5, pp. 2002–2041, Jun. 2020.

[48] L. Lu, P. Jin, G. Pang, Z. Zhang, and G. E. Karniadakis, "Learning nonlinear operators via DeepONet based on the universal approximation theorem of operators," *Nature Mach. Intell.*, vol. 3, no. 3, pp. 218–229, Mar. 2021.

[49] P. Ren, C. Rao, Y. Liu, J.-X. Wang, and H. Sun, "PhyCRNet: Physics-informed convolutional-recurrent network for solving spatiotemporal PDEs," *Comput. Methods Appl. Mech. Eng.*, vol. 389, Feb. 2022, Art. no. 114399.

[50] S. Bhardwaj and P. Gaire, "Data-free solution of electromagnetic PDEs using neural networks and extension to transfer learning," *IEEE Trans. Antennas Propag.*, vol. 70, no. 7, pp. 5179–5188, Jul. 2022.

MD RAYHAN KHAN (Member, IEEE) received the B.Sc. degree in electrical and electronic engineering from Bangladesh University of Engineering and Technology (BUET), Dhaka, Bangladesh, in 2016, and the M.S. degree in electrical engineering and the Ph.D. degree in electrical and computer engineering from Florida International University (FIU), Miami, FL, USA, in 2022 and 2023, respectively.

He was a Graduate Research Assistant with the Department of Electrical and Computer Engineering, FIU. His research interests include computational electromagnetics, antennas, antenna arrays, microwave circuits, optimization techniques, and machine learning.

CONSTANTINOS L. ZEKIOS (Senior Member, IEEE) received the Diploma degree (Hons.) in electrical and computer engineering, the M.S. degree (Hons.) in electrical and computer engineering communication and satellite telecommunication systems, and the Ph.D. degree (Hons.) in electrical and computer engineering from Democritus University of Thrace, Xanthi, Greece, in 2008, 2011, and 2015, respectively. He was a Postdoctoral Researcher with the Electrical and Computer Engineering Department, University of Massachusetts Amherst, Amherst, MA, USA, from January 2016 to May 2018, a Fellow Postdoctoral Researcher with the Transforming Antennas Center, Florida International University, Miami, FL, USA, from May 2018 to August 2020, and a Research Assistant Professor with the Department of Electrical and Computer Engineering, Florida International University, from September 2020 to July 2022. He is currently an Assistant Professor with the Department of Electrical and Computer Engineering, Florida International University. His main research interests include theoretical and computational electromagnetics, optimization methods, antennas and antenna arrays, electromagnetic surfaces, beamforming networks, microwave engineering, and photonics.

SHUBHENDU BHARDWAJ (Member, IEEE) received the B.Tech. degree (summa cum laude) in electronics engineering from IIT (ISM)-Dhanbad, India, in 2004, the M.S. degree from UCLA, CA, USA, in 2012, and the Ph.D. degree from The Ohio State University, Columbus, OH, USA, in 2017.

From 2008 to 2010, he was Samsung India Software Operations, Bangalore, India. He is currently an Assistant Professor with the Electrical and Computer Engineering Department, University of Nebraska–Lincoln, Lincoln, NE, USA. His current research interests include computational electromagnetics, wireless power harvesting, terahertz devices, and sub-mmwave/terahertz antennas. He is a recipient of the best student paper awards at URSIGASS-2017, IEEE-iWat-2017, and IEEE-AMTA-2015. His paper also received second place at the student paper competition at AMTA-2014 and honorable mentions at APS-2014 and 2015.

STAVROS V. GEORGAKOPOULOS (Senior Member, IEEE) received the Diploma degree in electrical engineering from the University of Patras, Patras, Greece, in June 1996, and the M.S. degree in electrical engineering and the Ph.D. degree in electrical engineering from Arizona State University (ASU), Tempe, AZ, USA, in 1998 and 2001, respectively.

From 2001 to 2007, he held a position as a Principal Engineer with SV Microwave Inc. Since 2007, he has been with the Department of Electrical and Computer Engineering, Florida International University, Miami, FL, USA, where he is currently a Professor, the Director of the Transforming Antennas Center (a research center on foldable/origami, physically reconfigurable and deployable antennas), and the Director of the RF Communications, Millimeter-Waves, and Terahertz Laboratory. His current research interests include novel antennas, arrays, RFID, microwave and RF systems, novel sensors, and wireless powering of portable, wearable, and implantable devices.

Dr. Georgakopoulos received the 2015 FIU President's Council Worlds Ahead Faculty Award, which is the highest honor FIU extends to a faculty member for excelling in research, teaching, mentorship, and service. He served as an Associate Editor of IEEE TRANSACTIONS ON ANTENNAS AND PROPAGATION, from 2013 to 2019, and IEEE OPEN JOURNAL OF ANTENNAS AND PROPAGATION, Since 2019.

• • •